Photoluminescence and low-threshold lasing of ZnO nanorod arrays

Ni Xu,[1] Yong Cui,[1] Zhigao Hu,[2] Wenlei Yu,[2] Jian Sun,[1] Ning Xu,[1] and Jiada Wu[1,*]

[1]*Department of Optical Science and Engineering, Fudan University, Shanghai 200433, China*
[2] *School of Information science & technology, East China Normal University, Shanghai 200241, China*
[*]*jdwu@fudan.edu.cn*

Abstract: We report on the photoluminescence (PL) and lasing characteristics of ZnO nanorod arrays (NRAs) fabricated by hydrothermal process on nanocrystalline ZnO seeded Si and post-growth annealing. The morphology of the ZnO NRAs was examined by field emission scanning electron microscopy and the structure was characterized by x-ray diffraction, Fourier-transform infrared and Raman scattering spectroscopy. The properties of light emission were studied by continuous wave (CW) and 30 ps pulsed ultraviolet excitation. The ZnO NRAs consist of aligned nanorods and are nanocrystalline with wurtzite structure and *c*-axis orientation. At room temperature, the ZnO NRAs are capable of emitting strong CW PL and pulsed stimulated emission, with the latter showing obvious lasing characteristics. The threshold for lasing was observed to be ~16 kW/cm^2.

OCIS codes: (140.3610) Lasers, ultraviolet; (140.5960) Semiconductor lasers; (160.4236) Nanomaterials; (160.6000) Semiconductor materials; (160.4760) Optical properties.

References and links

1. W. Wegscheider, L. N. Pfeiffer, M. M. Dignam, A. Pinczuk, K. W. West, S. L. McCall, and R. Hull, "Lasing from excitons in quantum wires," Phys. Rev. Lett. **71**(24), 4071–4074 (1993).
2. Z. K. Tang, M. Kawasaki, A. Ohtomo, H. Koinuma, and Y. Segawa, "Self-assembled ZnO nano-crystals and exciton lasing at room temperature," J. Cryst. Growth **287**(1), 169–179 (2006).
3. H. Cao, Y. G. Zhao, H. C. Ong, S. T. Ho, J. Y. Dai, J. Y. Wu, and R. P. H. Chang, "Ultraviolet lasing in resonators formed by scattering in semiconductor polycrystalline films," Appl. Phys. Lett. **73**(25), 3656–3658 (1998).
4. H. Cao, Y. G. Zhao, S. T. Ho, E. W. Seelig, Q. H. Wang, and R. P. H. Chang, "Random laser action in semiconductor powder," Phys. Rev. Lett. **82**(11), 2278–2281 (1999).
5. M. H. Huang, S. Mao, H. Feick, H. Q. Yan, Y. Y. Wu, H. Kind, E. Weber, R. Russo, and P. D. Yang, "Room-temperature ultraviolet nanowire nanolasers," Science **292**(5523), 1897–1899 (2001).
6. T. Okada, K. Kawashima, and M. Ueda, "Ultraviolet lasing and field emission characteristics of ZnO nano-rods synthesized by nano-particle-assisted pulsed-laser ablation deposition," Appl. Phys., A Mater. Sci. Process. **81**(5), 907–910 (2005).
7. Q. Li, K. Gao, Z. G. Hu, W. L. Yu, N. Xu, J. Sun, and J. D. Wu, "Photoluminescence and lasing properties of catalyst-free ZnO nanorod arrays fabricated by pulsed laser deposition," J. Phys. Chem. C **116**(3), 2330–2335 (2012).
8. L. Miao, S. Tanemura, Y. Ieda, M. Tanemura, Y. Hayashi, H. Y. Yang, S. P. Lau, B. K. Tay, and Y. G. Cao, "Synthesis, morphology and random laser action of ZnO nanostructures," Surf. Sci. **601**(13), 2660–2663 (2007).
9. E. S. Jang, X. Chen, J. H. Won, J. H. Chung, D. J. Jang, Y. W. Kim, and J. H. Choy, "Soft-solution route to ZnO nanowall array with low threshold power density," Appl. Phys. Lett. **97**(4), 043109 (2010).
10. H. Y. Yang, S. P. Lau, S. F. Yu, A. P. Abiyasa, M. Tanemura, T. Okita, and H. Hatano, "High-temperature random lasing in ZnO nanoneedles," Appl. Phys. Lett. **89**(1), 011103 (2006).
11. K. Okazaki, D. Nakamura, M. Higashihata, P. Iyamperumal, and T. Okada, "Lasing characteristics of an optically pumped single ZnO nanosheet," Opt. Express **19**(21), 20389–20394 (2011).
12. P.-H. Dupont, C. Couteau, D. J. Rogers, F. Hosseini Téhérani, and G. Lérondel, "Waveguiding-assisted random lasing in epitaxial ZnO thin film," Appl. Phys. Lett. **97**(26), 261109 (2010).
13. K. Gao, W. Zhang, J. Sun, N. Xu, Z. F. Ying, Q. Li, J. Gan, and J. D. Wu, "Influences of substrate and annealing on the structural and optical properties and photoluminescence of nanocrystalline ZnO films prepared by plasma assisted pulsed laser deposition," J. Phys. Chem. C **113**(44), 19139–19144 (2009).
14. B. D. Cullity and S. R. Stock, *Elements of X-ray Diffraction,* 3rd ed. (Prentice Hall Inc, 2001).
15. M. A. Verges, A. Mifsud, and C. J. Serna, "Formation of rod-like zinc oxide microcrystals in homogeneous solutions," J. Chem. Soc., Faraday Trans. **86**, 959–963 (1990).

#166230 - $15.00 USD Received 12 Apr 2012; revised 2 Jun 2012; accepted 7 Jun 2012; published 18 Jun 2012

16. T. C. Damen, S. P. S. Porto, and B. Tell, "Raman effect in zinc oxide," Phys. Rev. **142**(2), 570–574 (1966).
17. C. Y. Geng, Y. Jiang, Y. Yao, X. M. Meng, J. A. Zapien, C. S. Lee, Y. Lifshitz, and S. T. Lee, "Well-aligned ZnO nanowire arrays fabricated on silicon substrates," Adv. Funct. Mater. **14**(6), 589–594 (2004).
18. B. Q. Cao, W. P. Cai, H. B. Zeng, and G. T. Duan, "Morphology evolution and photoluminescence properties of ZnO films electrochemically deposited on conductive glass substrates," J. Appl. Phys. **99**(7), 073516 (2006).
19. W. Shan, W. Walukiewicz, J. W. Ager III, K. M. Yu, H. B. Yuan, H. P. Xin, G. Cantwell, and J. J. Song, "Nature of room-temperature photoluminescence in ZnO," Appl. Phys. Lett. **86**(19), 191911 (2005).
20. D. H. Fan, Z. Y. Ning, and M. F. Jiang, "Characteristics and luminescence of Ge doped ZnO films prepared by alternate radio frequency magnetron sputtering," Appl. Surf. Sci. **245**(1-4), 414–419 (2005).
21. B. P. Zhang, N. T. Binh, Y. Segawa, K. Wakatsuki, and N. Usami, "Optical properties of ZnO rods formed by metalorganic chemical vapor deposition," Appl. Phys. Lett. **83**(8), 1635–1637 (2003).
22. C. Klingshirn, *Semiconductor Optics,* 3rd ed. (Springer, 2007).

1. Introduction

With a wide direct band gap (~3.37 eV) and a large exciton binding energy (~60 meV) at room temperature, the exciton recombination in ZnO is expected to be a more effective radiative process compared with the electron-hole process and makes ZnO capable of realizing low-threshold UV lasing performance [1,2]. Since the first reports on the random lasing action in disordered ZnO polycrystalline films and powders by Cao *et al*. [3,4], lasing characteristics of different structures of ZnO have attracted much attention. Due to the expected low threshold required for lasing in ZnO structures in reduced dimensionality, lasing in nanostructured ZnO is of particular interest, and lasing behaviors have been demonstrated in various types of ZnO nanostructures including nanorods [5–7], nanowalls [8,9], nanoneedles [10] and nanosheets [11].

Although the lasing action based on excitonic recombination in ZnO is expected to be efficient, it has been proved that a high pump power, usually at the order of 10^5 W/cm^2 and above, is necessary for achieving UV lasing in the case of optical pumping. For an epitaxial ZnO thin film, a typical lasing threshold of 900 kW/cm^2 was identified [12]. The threshold of ZnO nanostructures is strongly dependent on the morphology of nanostructure [8]. Miao *et al*. observed optically pumped random lasing in ZnO random-wall arrays with a threshold of 0.38 MW/cm^2 [8]. Okazaki *et al*. demonstrated that ZnO nanosheets have a lower threshold (~50 kW/cm^2) than that of ZnO nanowires (~150 kW/cm^2) [11]. Recently, a considerably low threshold (~25 kW/cm^2) of ZnO nanowall arrays optically pumped by a frequency-tripled Q-switched YAG laser was reported [9]. Yang *et al*. reported that for random lasing in ZnO nanoneedles, the lasing threshold also depended on temperature, and it increased from ~0.25 MW/cm^2 at 300 K to ~2.05 MW/cm^2 at 615 K [10]. In this work, we report on the lasing characteristics of well-aligned ZnO nanorod arrays (NRAs) hydrothermally grown on nanocrystalline ZnO (NC-ZnO) seeded Si substrates. With optical pumping by UV laser pulses, clear stimulated emission was observed from 600 °C annealed ZnO NRAs at a pump intensity of about 16 kW/cm^2. The fabricated ZnO NRAs were also characterized for structure and continuous wave (CW) photoluminescence (PL) studies.

2. Experimental details

N-type Si (100) wafers were used as the substrates after being chemically cleaned. ZnO NRAs were fabricated by two-step process. Prior to the growth of ZnO nanorods, a thin (~20 nm) NC-ZnO film was deposited on the Si substrate by plasma assisted pulsed laser deposition [13] and annealed at 400 °C in air for 1 h. The annealed NC-ZnO film served both as the buffer layer between lattice mismatched ZnO and Si and as the seed layer which assisted the nucleation of ZnO and the growth of ZnO nanorods. The NC-ZnO seeded Si substrate was immersed into a hydrothermal precursor solution which was prepared by mixing 0.04 M hexamethylenetetramine (HMT) and 0.04 M zinc nitrate hexahydrate [$Zn(NO_3)_2{\cdot}6H_2O$] into 1 L de-ionized water. The hydrothermal growth was carried out at 90 °C in a thermostatic water bath for 6 h. All the chemicals were ≥ 99.0% in purity and used as purchased without further purification. After growth, the samples were washed with de-ionized water, dried in air at room temperature, and then annealed at 600 °C in N_2 for 1 h.

#166230 - $15.00 USD Received 12 Apr 2012; revised 2 Jun 2012; accepted 7 Jun 2012; published 18 Jun 2012

The morphology of the fabricated ZnO NRAs was examined by field emission scanning electron microscopy (FESEM) with a Hitachi S-4800 microscope. The crystal structure of the ZnO nanorods was characterized by x-ray diffraction (XRD) with a Rigaku D/MAX 2550 VB/PC x-ray diffractometer using Ni-filtered Cu Kα radiation. Fourier-transform infrared (FTIR) spectroscopy and Raman scattering spectroscopy were performed for bonding analysis and phase identification. FTIR spectroscopy was carried out with a Bruker Vertex 80V spectrometer. Raman measurements were performed with a Jobin-Yvon LabRAM HR 800 UV micro-Raman spectrometer using 488 nm and 325 nm laser beams to excite the samples.

CW PL measurements were carried out at temperatures ranging from 10 to 300 K by exciting the samples normally with 325 nm He-Cd laser and collecting the luminescence also at the normal direction. The luminescence was dispersed by a 0.5 m spectrometer (Acton, Spectra Pro 500i) and detected by an intensified charge-coupled device (Andor, iStar DH720). Room temperature lasing properties were studied by optically pumping the samples at normal incidence with 355 nm and 30 ps laser pulses of the frequency-tripled output from a mode-locked Nd: YAG laser working at 10 Hz. The emitted light was detected nearly perpendicular to the sample surface and recorded with an exposure time of 5 seconds by a charge-coupled device (Andor, DV401-BV) in combination with an Acton Spectra Pro 2750 spectrometer.

3. Results and discussion

3.1 Morphology and structure

FESEM examination revealed that the ZnO nanorods grew nearly vertically and had hexagonal shapes with well-faceted surfaces both at the ends and sides. No obvious changes were observed in the morphology after annealing. Figure 1 shows the planar and cross-sectional FESEM images of the annealed samples. It can be seen that hexagonal ZnO nanorods with typical diameters of 80 to 120 nm were fabricated. Except near the front edge of the cross-sectional FESEM image where some nanorods were broken when cutting the sample for cross-sectional FESEM examination, the fabricated samples have a flat-surface appearance, indicating that the grown nanorods roughly have the same length of ~1.5 μm. Approximately shaped with hexagonal prism, the nanorods are highly oriented with their axes perpendicular to the substrate and are generally separated from each other from the bottom to the top with almost the same density, forming a well-aligned nanorod array.

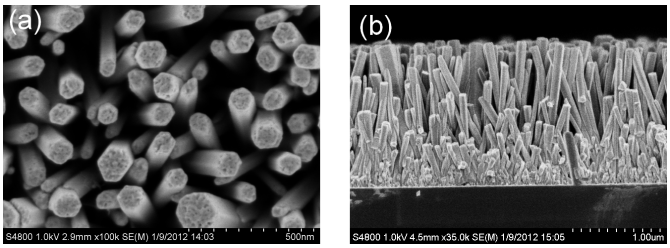

Fig. 1. FESEM images of annealed ZnO NRAs: (a) planar image; (b) cross-sectional image.

Figure 2(a) shows the XRD patterns of the fabricated ZnO NRAs. Besides the diffraction from the Si substrate, the dominant peak is identified as the (002) diffraction of hexagonal wurtzite ZnO for the as-grown sample, suggesting that the ZnO nanorods grew with the preference of (002) orientation along the *c*-axis perpendicular to the substrate. The XRD pattern also reveals the presence of orientations other than the dominant *c*-axis orientation. After annealing, the diffraction intensities increase significantly, except the (100) peak which can hardly be identified. The increase in diffraction intensities, especially the (002) diffraction for which the narrowing in diffraction peak was also observed, indicates the improvement in ZnO crystallinity. For the annealed sample, the (002) diffraction of wurtzite ZnO dominates the XRD pattern, which peaks at $2\theta_{002} = 34.55°$ with a full width at half-maximum (FWHM) of 0.18°, also implying good crystal quality of the annealed ZnO nanorods. Another prominent peak at $2\theta_{103} = 63.07°$, indexed to the (103) diffraction of wurtzite ZnO, also

#166230 - $15.00 USD Received 12 Apr 2012; revised 2 Jun 2012; accepted 7 Jun 2012; published 18 Jun 2012

increases after annealing. But the increase of the (103) diffraction is not so significant as the (002) diffraction. The lattice constants were determined to be a = 0.324 nm and c = 0.519 nm, respectively, for the annealed sample. The measured diffraction patterns and the calculated lattice constants suggest that the ZnO nanorods on the NC-ZnO seeded Si (100) substrate are almost stress free after annealing. Moreover, the XRD characterization also reveals that the ZnO nanorods are nanocrystalline. The mean size of the crystallites was calculated to be 46 nm using the Scherrer's formula [14]. The fabricated nanorods are therefore not single crystal in structure, but are composed of crystallites with an average size of 46 nm.

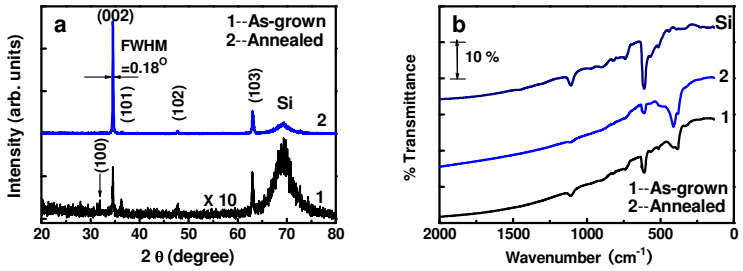

Fig. 2. (a) XRD patterns of as-grown and annealed ZnO NRAs. For clarity, the XRD pattern taken from as-grown ZnO nanorod arrays is magnified by 10 times. (b) FTIR spectra recorded for as-grown and annealed ZnO NRAs. FTIR spectrum recorded for Si (100) substrate is also shown for comparison.

FTIR measurements confirmed the formation of ZnO phases. The FTIR transmission spectra recorded for the ZnO NRAs in the wavenumber region below 2000 cm^{-1} are displayed in Fig. 2(b) together with that recorded for the Si substrate as a reference. Besides the absorptions of the Si substrate, the principal IR absorptions of the as-grown ZnO NRAs are in the wavenumber range from 345 to 455 cm^{-1}, with one absorption peaking at 380 cm^{-1} and another one appearing as a shoulder around 415 cm^{-1}. Zinc oxide presents a wurtzite structure with two transverse optical modes at $\omega_{T//}$ = 377 cm^{-1} and $\omega_{T\perp}$ = 406 cm^{-1}, whose position and intensity are affected by the morphology and structure in microcrystalline samples [15]. The observed IR absorptions near 380 and 415 cm^{-1} for the as-grown ZnO NRAs could be assigned to the stretching mode of Zn–O–Zn. For the annealed sample, a slight broadening in absorption band was observed with the absorption near 415 cm^{-1} increasing significantly and becoming stronger than the one near 380 cm^{-1}. In addition, the relative intensity of the absorptions attributed to ZnO to those attributed to the Si substrate increases after annealing, which could be associated with the improvement in the ZnO crystallinity due to annealing.

Raman scattering measurements provide convincing supports for the wurtzite structure of the prepared ZnO nanorods and the improvement in crystallinity of ZnO by annealing. For hexagonal wurtzite ZnO, the non-polar phonon modes E_2 have low- and high-frequency components, and the polar A_1 and E_1 modes split into longitudinal optical (LO) and transverse optical (TO) components. Therefore, wurtzite ZnO has six Raman active phonon modes E_2 (low), E_2 (high), A_1 (TO), A_1 (LO), E_1 (TO), and E_1 (LO) [16,17]. Figure 3(a) represents the Raman spectra taken from the fabricated samples at 488 nm light excitation. Comparing with the Raman spectrum recorded for the Si substrate, it seems no obvious Raman signals scattered from ZnO for the as-grown sample. After annealing, the sample exhibit very different Raman features. Two strong and sharp peaks are prominent at 99 and 438 cm^{-1} with their FWHMs of about 2.5 and 8 cm^{-1}, respectively. They are corresponding to the E_2 (low) and E_2 (high) modes. The strong E_2(low) and E_2(high) peaks demonstrate that the annealed ZnO nanorods are of good crystalline hexagonal structure. The high crystalline quality is also indicated by the very narrow linewidths of these two peaks [17]. Weak peaks attributed to wurtzite ZnO can also be identified at around 330, 375 and 579 cm^{-1}. The former can be

#166230 - $15.00 USD Received 12 Apr 2012; revised 2 Jun 2012; accepted 7 Jun 2012; published 18 Jun 2012

assigned to a second-order optical mode of hexagonal ZnO ($^2E_2$) [18], the middle to the A_1 (TO) mode [18], while the latter most probably consists of the A_1 (LO) and the E_1 (LO) modes [16]. By exciting the samples with 325 nm laser beam, the resonant Raman spectra of the ZnO nanorods show multiphonon LO modes up to the third order, as displayed in Fig. 3(b). For the as-grown ZnO nanorods, three prominent peaks at 572, 1145, and 1723 cm^{-1} were observed with their bandwidths increasing, which mainly result from the polar symmetry modes A_1(LO) and E_1(LO) and their overtones. In addition, a broad band appears as a shoulder, which is attributed to the scattering corresponding to the E_2 (high) mode. After annealing, the E_2 (high) scattering becomes more intense, consistent with the results obtained by conventional Raman measurements with visible light excitation.

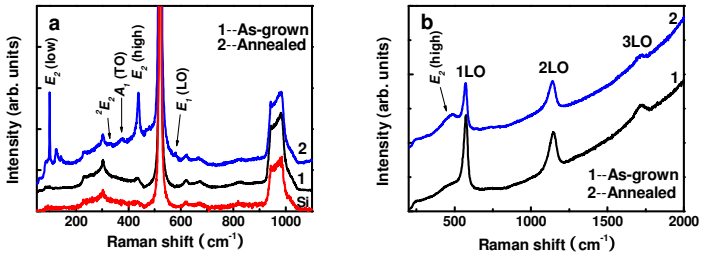

Fig. 3. Raman spectra of prepared ZnO NRAs excited by 488 nm (a) and 325 nm (b) laser beam.

3.2. Photoluminescence

Room temperature CW PL spectra of the fabricated ZnO NRAs are shown in Fig. 4(a). For the as-grown samples, the dominant emission peeks at 376 nm with an FWHM of 14 nm. This UV luminescence is attributed to the room-temperature free exciton related near-band-edge (NBE) emission in ZnO [19], as will be verified by temperature-dependent PL measurements. Besides the NBE luminescence, weak and broad visible luminescence centered at 560 nm was also observed with its intensity about 3% of the NBE emission intensity. The green luminescence is usually believed to be associated with oxygen vacancies related to structural defects [20]. The weak visible luminescence suggests the low concentration of oxygen vacancies in the as-grown ZnO nanorods. For the annealed ZnO NRAs, the UV NBE luminescence increases by 30% in its intensity, resulting from the improvement in crystal qualities of the ZnO nanorods. However, the green luminescence becomes even weaker and could hardly be observed (less than 0.5% of the NBE luminescence intensity), as shown by the inset of Fig. 4(a). The almost absence of the defect-related visible luminescence indicates that the concentrations of such defects are negligible in the annealed sample, again indicating the improvement in structure due to annealing.

As a result of the freeze-out of phonons and quenching of nonradiative recombination processes at low temperatures, the NBE luminescence increases significantly with a remarkable blue shift and a much narrower width. Figure 4(b) compares the PL spectra recorded at 10 K and 300 K for the as-grown ZnO NRAs. The NBE luminescence shifts to 367.9 nm with an FWHM of 2.4 nm. This luminescence results from the radiative decays from a number of free and bound exciton complexes. The inset in Fig. 4(b) illustrates the details of the NBE luminescence associated with the emissions attributed to various excitons and their phonon replicas. The strongest emission peaks at 3.370 eV with its FWHM of 22 meV, which is attributed to bound excitonic emission at neutral donors (D^0X) [19], revealing that bound exciton emissions are the dominant radiative recombination channels at low temperatures. The emission associated with free excitons (FX) appears as a shoulder at the higher energy side of the D^0X peak. The D^0X peak is also accompanied at the low energy side by an emission at 3.348 eV, which can be attributed to the neutral-acceptor bound excitons

#166230 - $15.00 USD Received 12 Apr 2012; revised 2 Jun 2012; accepted 7 Jun 2012; published 18 Jun 2012

(A^0X). In addition to the emissions associated with bound and free excitons, another PL band is clearly resolved at 3.324 eV. It is most likely from the radiative recombination processes arising from donor-to-acceptor (DAP) pair transitions [21].

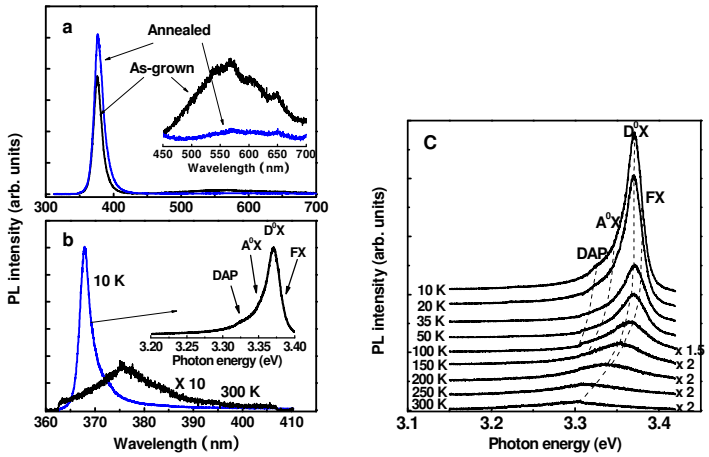

Fig. 4. (a) Room temperature PL spectra of as-grown and annealed ZnO NRAs. (b) PL spectra of as-grown ZnO NRAs recorded at 300 and 10 K. The inset shows the details of the PL recorded at 10 K. (c) Temperature-dependent PL spectra in the near band edge region taken from as-grown ZnO NRAs.

Figure 4(c) displays the temperature-dependent PL of the as-grown ZnO NRAs at temperatures from 10 to 300 K. It can be seen that as the temperature increases, the luminescence including all its components shows an obvious red shift. Moreover, the PL intensity decreases rapidly, especially for the emission associated with donor bound excitons which decreases much faster and gradually loses its dominance, revealing the release of excitons from donors. In contrast, the free exciton associated emission decreases much slower. Such an evolution of the PL features with temperature is attributed to the decomposition of bound excitons to free ones with increasing the thermal energy. When the temperature is raised to about 200 K, the free exciton emission dominates the NBE luminescence while the bound exciton emission becomes hardly resolvable, suggesting the complete decomposition of bound excitons to free ones. The dependence of the PL features on temperature and the transition from the bound exciton emission dominating luminescence to the free exciton dominating one obviously reveal that the dominant room-temperature NBE luminescence results from the radiative recombination of free excitons.

3.4 Lasing Emission

The strong predominant NBE exciton luminescence suggests that the fabricated ZnO NRAs have excellent room-temperature lasing characteristics, which were verified by optically pumping. At low pump powers, only a broad spontaneous emission can be observed. The increase of the pump power results in the emergence of discrete sharp peaks superposed on the broad featureless emission. Figure 5(a) shows the evolution of the emission spectra of the as-grown ZnO NRAs as the pump intensity increases. Additional narrow peak at 381 nm emerges when the power intensity exceeds 20 kW/cm^2, suggesting the approach of threshold for lasing and the transition from spontaneous emission to stimulated one. With the pump power further increasing, the number and the intensity of the lasing peaks also increase. For the annealed ZnO NRAs, a lower threshold for lasing was observed. Figure 5(b) illustrates the evolution of the emission spectra of the annealed ZnO NRAs as a function of pump power. At a pump intensity of ~16 kW/ cm^2, several discrete peaks emerge, suggesting the occurrence of

#166230 - $15.00 USD Received 12 Apr 2012; revised 2 Jun 2012; accepted 7 Jun 2012; published 18 Jun 2012

the lasing action in the ZnO NRAs. The decrease of threshold for lasing in the annealed sample could be attributed to the improvement in crystal structure and oxide phases of the ZnO nanorods by annealing. As the pump intensity increases, the intensity of discrete peaks increases dramatically together with the appearance of more lasing peaks.

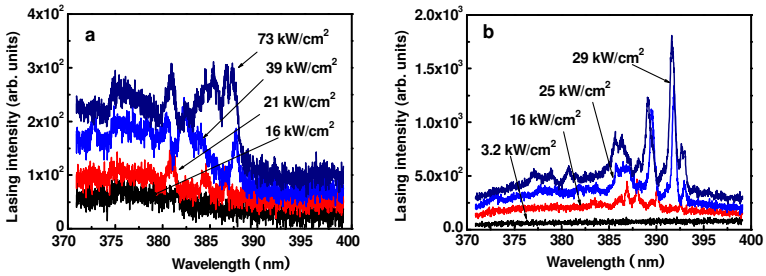

Fig. 5. Spontaneous and lasing emission spectra obtained at different pump intensities taken from (a) as-grown and (b) annealed ZnO nanorod arrays.

It is worthwhile noting that the linewidths of the sharp peaks are very narrow (FWHM ~0.6 nm) and the spacings between the adjacent sharp peaks are not the same, which resembles a spectrum resulting from a random lasing process. In nanostructured ZnO materials, ZnO can provide optical amplification as a gain medium and light forms close loops by multiple scattering. These loops can serve as laser resonators. For a ZnO nanorod, it can act both as a laser resonator for guided modes and as a gain medium for stimulated emission [22]. The lasing emission wavelength is defined by the guided modes of the nanorod. In our case, however, the ZnO NRA is an ensemble of nearly aligned ZnO nanorods with different sizes. The discrete peaks of the emission from the sample represent a superposition of lasing modes from different ZnO nanorods, rather than the lasing due to photon coherent scattering. The emission wavelengths of lasing modes of each nanorod in the ensemble do not coincide exactly with each other. Therefore, the emitted lasing emission on the whole looks much like as random lasing rather than well defined one. It is also worth mentioning that the observed threshold is much lower than the early reported value for the ZnO nanorod arrays prepared by pulsed laser deposition [7]. We have noticed that in that case, the nanorods were irregular with different shapes and sizes, and grew densely with their diameters gradually decreasing from the bottom to the tip. In the present work, in contrast, highly aligned hexagonal ZnO nanorods were fabricated with well-faceted surfaces both at the ends and sides. ZnO nanorods with more perfect shape are more effective acting as resonators and gain mediums for stimulated emission, and hence low-threshold lasing can be expected.

4. Conclusions

We have demonstrated low-threshold lasing in ZnO nanorod arrays fabricated hydrothermally on nanocrystalline ZnO seeded Si. The nanorods are vertically aligned with typical diameters of 80 to120 nm and a length of 1.5 μm and are nanocrystalline with wurtzite structure and *c*-axis orientation. At room temperature, the ZnO NRAs exhibit good behaviors on UV luminescence with CW light excitation and UV lasing emission with 30 ps optical pumping. Annealing in N_2 results in an improvement in ZnO crystallinity and an enhancement in light emission. The lasing threshold power density of the annealed ZnO NRAs is ~16 kW/cm^2. The random-lasing-like emission is a superposition of guided lasing modes from an ensemble consisting of ZnO nanorods with different sizes. The remarkable performance on UV emission is attributed to the oriented alignment of ZnO nanorods with high crystalline quality.

Acknowledgments

This work is supported by the National Basic Research Program of China (No. 2012CB934303) and the Doctoral Fund of Ministry of Education of China (No. 20110071110020). Acknowledgment is also made to the Natural Science Foundation of China.

#166230 - $15.00 USD Received 12 Apr 2012; revised 2 Jun 2012; accepted 7 Jun 2012; published 18 Jun 2012